Environ. Sci. Technol. **2009,** *43,* 5436–5442

Evaluation of Intracellular Polyphosphate Dynamics in Enhanced Biological Phosphorus Removal Process using Raman Microscopy

NEHREEN MAJED,[†] CHRISTIAN MATTHÄUS,[‡] MAX DIEM,[‡] AND APRIL Z. GU*,[†]

Department of Civil and Environmental Engineering, 360 Huntington Avenue, Northeastern University, Boston, Massachusetts 02115, and Department of Chemistry and Chemical Biology, 360 Huntington Avenue, Northeastern University, Boston, Massachusetts 02115

Received January 30, 2009. Revised manuscript received May 6, 2009. Accepted May 11, 2009.

A Raman microscopy method was developed and successfully applied to evaluate the dynamics of intracellular polyphosphate in polyphosphate-accumulating organisms (PAOs) in enhanced biological phosphorus removal (EBPR) processes. Distinctive Raman spectra of polyphosphates allowed for both identification of PAOs and quantification of intracellular polyphosphate during various metabolic phases in a lab-scale EBPR process. Observation of polyphosphate at individual cell level indicated that there are distributed states of cells in terms of polyphosphate content at any given time, suggesting that agent-based distributive modeling would more accurately reflect the behavior of an EBPR process than the traditional average-state based modeling. The results, for the first time, showed that the polyphosphate depletion or replenishment observed at the overall population level were collective results from shifts/transition in the distribution of abundance of PAOs with different amounts of polyphosphate inclusions during EBPR. Imaging construction based on simultaneous quantification of intracellular polyphosphate and protein revealed the spatial distribution of polyphosphate inside cells and showed that the polyphosphates accumulate in smaller or larger aggregates, rather than being evenly distributed within the cytoplasm. The results demonstrated that Raman microscopy will allow for detailed cellular-level evaluation of polyphosphate metabolism and dynamics in EBPR processes and revealed mechanism insights, which otherwise would not be obtained using a traditional bulk measurement-based approach.

Introduction

Enhanced biological phosphorus removal (EBPR) is a widely applied process in wastewater treatment for removing phosphorus to control eutrophication in receiving waters. Successful EBPR processes rely on the selection of polyphosphate accumulating organisms (PAOs), which are able to store intracellular polyphosphates, poly hydroxyalkanoates (PHAs), and glycogen polymers as energy and carbon sources (*1*). Under anaerobic conditions, PAOs use the energy generated from the cleavage of polyphosphates and reducing power from glycolysis of glycogen to uptake available carbon sources such as volatile fatty acids (VFAs) and store them as PHAs; and under the subsequent aerobic/anoxic conditions, PAOs use their stored PHAs as energy and carbon sources for biomass growth, glycogen replenishment, phosphate uptake and polyphosphate restorage. Net phosphate removal from the wastewater is achieved via the wasting of the sludge containing high phosphate content. This unique metabolic system in PAOs provides them with the selective advantage to thrive in the EBPR system in wastewater treatment.

Currently, little is known about the composition, structure, and length of intracellular polyphosphates and their potential impact on the phosphate removal function of PAOs. Phosphate polymers consist of chains of phosphate and electron counter-balancing cations, such as hydrogen (H+), magnesium (Mg^{2+}), potassium (K^{+}), and calcium (Ca^{2+}) (*2*). Schönborn et al. (*3*) showed that many types of polyphosphate granules with different Mg^{2+}/P, K^{+}/P, and Ca^{2+}/P mole ratios can coexist. Lindrea et al. (*4*) and Lockwood et al. (*5*) showed that the form and length of polyphosphates (short-chain (SCP), long-chain (LCP), and granular polyphosphates) and associated counter-cations among different length cellular polyphosphates fractions in EBPR sludge depended on EBPR process configuration and the amount of nitrate returned to the anaerobic zone. The LCPs seemed to be associated with more stable performance with less nitrate return (*4*). All these observations indicate that the polyphosphate structure and composition may vary among different EBPR systems and they may affect the phosphate removal performance and stability. Investigation of microscale intracellular polyphosphate composition and dynamics and their impact on macro-scale phosphate removal will improve our understanding of the function of PAOs and allow us to better design and predict the performance of EBPR processes.

Cellular inclusion of polyphosphates can be qualitatively detected through staining techniques, such as Neisser and 4′,6-diamidino-2-phenylindole (DAPI) stains (*6*). However, the quantity and variation of polyphosphates in each cell, its dynamic association with different EBPR conditions, and the composition as well as structures of polyphosphate associated with different PAO populations have never been investigated. It is known that polyphosphate is a linear polymer of orthophosphate monomers to produce either linear or circular chains (*7*). The degree of polymerization, for activated sludge, could vary from 3−20 monomer units of acid-soluble fractions to a higher number of units of acid-insoluble fractions (*8*). Extractions of polyphosphates of different chain lengths have been performed before, but are rather time-consuming and involve complex analytical procedures (*4, 5*).

Recent developments in combining Raman spectroscopy with optical microscopy provide a new noninvasive technique to assess and, to a certain extent, image biochemical compositions of individual prokaryotes. Raman spectroscopy is based on inelastic light scattering events between a photon and a molecule that results in the excitation of molecular vibrations. Raman spectra contain information about chemical composition, bonding, symmetry, structures, and physical parameters (*9*). The coupling of a Raman spectrometer to a microscope makes it possible to study the chemical nature of a sample at submicrometer spatial resolution and has great potential for widespread applications in microbiology.

* Corresponding author e-mail: april@coe.neu.edu.
[†] Department of Civil and Environmental Engineering.
[‡] Department of Chemistry and Chemical Biology.

10.1021/es900251n CCC: $40.75

Published on Web 06/03/2009

Raman microscopy has been employed to identify and distinguish bacterial types and strains, to study heterogeneities in microbial colonies, to study the uptake of isotopically labeled nutrients and toxins in groundwater microorganisms, and to gain information on the chemical composition of bacteria (*9*−*12*).

In this study, we have investigated the application of Raman microscopy for evaluating single-cellular-level structural information and quantification of polyphosphates in PAOs enriched in a lab-scale EBPR process. The objective of this study is to develop a Raman microscopy method to identify and quantify polyphosphates in individual PAO cells in a mixed culture and apply it to elucidate the cellular-level polyphosphate dynamics associated with various metabolic conditions in an EBPR process. We believe that Raman microscopy is ideal to study polyphosphate accumulation at the single-cell level and may provide detailed insight into the dynamics of the metabolism of these organisms, which has advantages over techniques that measure only concentrations of bulk quantities.

Experimental Methodology

Enrichment of PAOs in Laboratory-Scale EBPR Process. Currently identified groups of microorganisms known to be active in EBPR include *Accumulibacter* in the *Betaproteobacteria*, *Actinobacteria*, and others (*13*). However, no isolated PAOs have yet been obtained. A laboratory-scale continuous-flow EBPR system was established to evaluate P removal performance and enrich for PAOs that could be used for the analysis of polyphosphate inclusions inside the cells. The reactor includes an anaerobic zone and an anoxic zone, followed by two-stage aerobic zones; the configuration allows for both A2O (anaerobic−anoxic−oxic) and UCT (University of Cape Town) mode of operation. The HRT and SRT of the system were maintained at 18 h and 8 days, respectively. The composition of synthetic wastewater feed was prepared according to Schuler and Jenkins (*14*). Phosphorus was added as 35.6 mg/L sodium phosphate monobasic ($NaH_2PO_4 \cdot H_2O$) (8 mg P/L). The organic portion of the feeding consisted of 744 mg/L sodium acetate ($CH_3COONa \cdot 3H_2O$) (350 mg COD/L) and 15 mg/L of casamino acids.

Presence of PAOs in the reactor was confirmed with phosphate removal performance evaluation, Neisser staining, and fluorescence in situ hybridization (FISH). Oligonucleotide probes including PAO651, PAO846, and PAO462 (*15*) were used to identify and quantify *Accumulibacter* type PAOs, and EUB338 probe (*16*) was used for counting the total cellular abundance. The PAOs in the reactor seemed to have signature grape-like cocci morphology and they were relatively large in size (3−5 μm) in comparison to other bacterial cells.

Raman Microscopy and Spectra Acquisition. Raman spectra were acquired using a WITec, Inc. (Ulm, Germany) model CRM 2000 confocal Raman microscope. Excitation (ca. 30 mW at 633 nm) was provided by a helium/neon laser (Melles Griot, Carlsbad, CA). The exciting laser radiation was coupled into a Zeiss microscope through a wavelength-specific single mode optical fiber. The incident laser beam was collimated via an achromatic lens and passed a holographic band-pass filter, before it was focused onto the sample through the microscope objective. A Nikon Plan (100*x*/0.9 NA, WD = 0.26 mm) air objective was used in the studies reported here. For single-point spectra the illumination time was 5 s. The sample was located on a piezo-electrically driven microscope scanning stage with an *x*,*y* resolution of ca. 3 nm and a repeatability of ±5 nm, and *z* resolution of ca. 0.3 nm ± 2 nm repeatability. For imaging, the sample was scanned through the laser focus in a raster pattern at a constant stage speed of fractions of a micrometer per second. Spectra were collected at a 0.33 μm grid, with a dwell time of 1 s. Relative quantity of polyphosphate content in each individual cell was evaluated based on the Raman intensity (peak height in the unit of charged coupled device (CCD) counts) of the PO_2^- stretching band occurring around 1168−1175 cm^{-1} wavenumber region after background correction.

Raman Spectra of Phosphates Standards. Raman spectra were recorded and compared for three phosphate standards: sodium phosphate monobasic ($NaH_2PO_4 \cdot H_2O$), sodium pyrophosphate ($Na_4P_2O_4 \cdot 10H_2O$), and sodium hexa-meta phosphate ($(NaPO_3)_6$). Chemicals were obtained from Sigma Chemical Company (Montana). Polyphosphates of higher molecular weight than the hexamer could not be obtained commercially.

Raman Spectra of Polyphosphates in PAOs. Raman spectra of cells in the mixed culture were examined to identify PAO cells that exhibit characteristic peaks of polyphosphates (determined based on polyphosphates standards and literature). To further confirm the identification of characteristic spectra of polyphosphates in PAOs, a correlation of the abundance of PAO cells (based on polyphosphate spectra) and phosphate concentration in solution during the phosphate uptake and release tests was evaluated. Details of phosphate release and uptake tests can be found elsewhere (*17*). The batch testing in this particular study consisted of 180 min anaerobic phase with acetate addition (100 mg COD/L) followed by 180 min aerobic phase. For polyphosphate detection using Raman microscopy, at least 6 samples were taken throughout the test at 45−90 min intervals. The batch testing samples were analyzed for Raman response and for chemical analysis. Each sample (10 mL) was filtered through 0.45-μm filter papers and analyzed for PO_4^{3-}, TOC, and COD using a DX-120 ion chromatograph, a Tekmar/Dohrmann Phoenix 8000 UV-Persulfate TOC analyzer, and HACH COD vials, respectively.

Samples were prepared on optically polished CaF_2 windows (Wilmad LabGlass, Buena, NJ). A 1-mL portion of unfiltered sample was collected in a micro centrifuge tube and then disrupted with 26 gauge needle and syringe for 20 times for uniform distribution of cells. Then 10−20 μL of sample was spread on the CaF_2 slides. Raman spectra for at least 25−30 single cells were examined for each sample.

Results and Discussion

Raman Spectra of Polyphosphates of Different Chain Length. Figure 1A shows a Raman spectrum of the orthophosphate ($NaH_2PO_4 \cdot H_2O$) salt. The two peaks of high intensity at 907 and 975 cm^{-1} can be assigned to the symmetric and antisymmetric P−O stretches. In solution, the symmetry of the molecule is pH dependent and the two peaks merge into one centered at 891 cm^{-1}, if the third oxygen is hydrogenated at lower pH values (*18*). Of less intensity is the $P{=}O$ stretch at 1175 cm^{-1}. The spectra of pyro-phosphate ($Na_4P_2O_7 \cdot 10H_2O$) and hexa-meta-phosphate ($(NaPO_3)_6$) are shown in Figure 1B and C, respectively. The spectrum of the dimer is dominated by the P−O−P stretching of the phosphate ester linkage at 738 cm^{-1} and the symmetric stretches of the PO_3^{2-} moieties at 1022 cm^{-1}. Similarly, for the spectrum of the hexamer, the P−O−P vibrations are shifted to 690 cm^{-1} because of the increase in polymer chain lengths, whereas the PO_2^- stretches of the ester chain are shifted to higher wave numbers at 1157 cm^{-1} due to the decrease in conjugation of the phosphate bonds. This is consistent with previous observations that for amorphous polyphosphate the P−O−P and PO_2^- bands are at 690 and 1151 cm^{-1}, respectively (*18*). Increase in polyphosphate ester chain length is expected to further move the P−O−P stretching band to lower wavenumbers (*19*) and move the PO_2^- stretching band to higher wavenumbers as has been observed for the Raman spectra of the phosphate oligomers. Unfortunately, polyphosphates of molecular weight higher

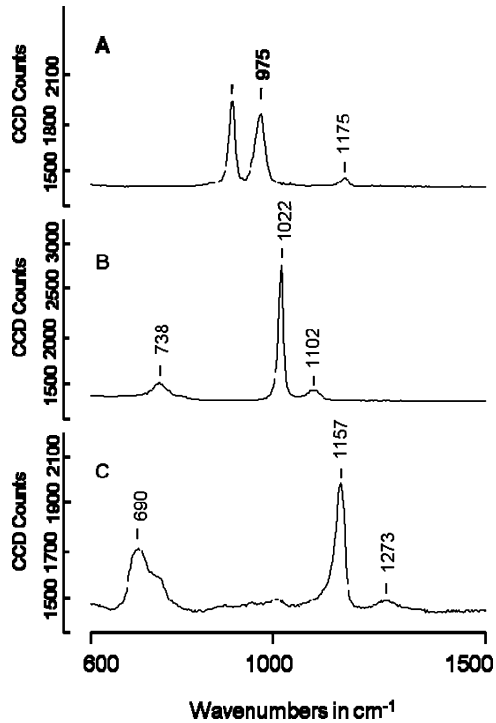

FIGURE 1. Raman spectra of (A) ortho-phosphate ($NaH_2PO_4 \cdot H_2O$), (B) pyro-phosphate ($Na_4P_2O_4 \cdot 10H_2O$), and (C) hexa-meta-phosphate ($(NaPO_3)_6$).

than hexamer are not commercially available for Raman study. It has been suggested that it is impossible to distinguish between different polyphosphates at longer polymer chains length using Raman spectroscopy due to the broad appearance of the P−O−P bands in the same spectral region for polyphosphates of different chain length (*18*). Nevertheless, the standards of polyphosphate pointed out the wavenumber regions of the signature peaks associated with polyphosphate.

Raman Spectra of Polyphosphates and Cellular Molecules in PAOs. Examination of Raman spectra of cells from the reactor led to the identification and differentiation of PAOs with distinct polyphosphate peaks from non-PAOs or PAOs without any polyphosphate peaks. Figure 2A and B show the Raman spectra for a PAO cell with polyphosphate and that for a bacterium without polyphosphate inclusions, respectively. The two phosphate peaks at 1175 and 700 cm^{-1} are superimposed with the spectral features of the proteins of the bacterium and are of considerably high intensities. The center peak positions of the PO_2^- vibrations varied from 1168 to 1177 cm^{-1} at higher wavenumber regions compared to the hexamer at 1157 cm^{-1}. And also the peak positions varied from 690 to 700 cm^{-1} for the P−O−P stretches, which is almost the same as the hexamer at 690 cm^{-1}. Thus, considering the combined shift, it is suggestive that polyphosphate chains are longer than the hexamer in the PAO cells. Although further investigation on how to differentiate polyphosphate with longer chain lengths is needed, it is clear that the two distinctive polyphosphate peaks of Raman spectra allow for identification of PAO cells in our EBPR system.

Raman spectra of bacteria have been reported for many types and strains. In general the spectra reflect the overall biochemical composition and the most prominent peaks can be assigned to vibrations of the protein backbones and their individual residues (*11, 20*). The most pronounced Raman intensities between 2800 and 3050 cm^{-1} originate from C−H stretching vibrations of the organic molecules of the organism. The spectral region between 1800 and 700 cm^{-1}, often called the fingerprint region, is dominated by several protein bands. The C═O stretching vibrations of the carbonyl group

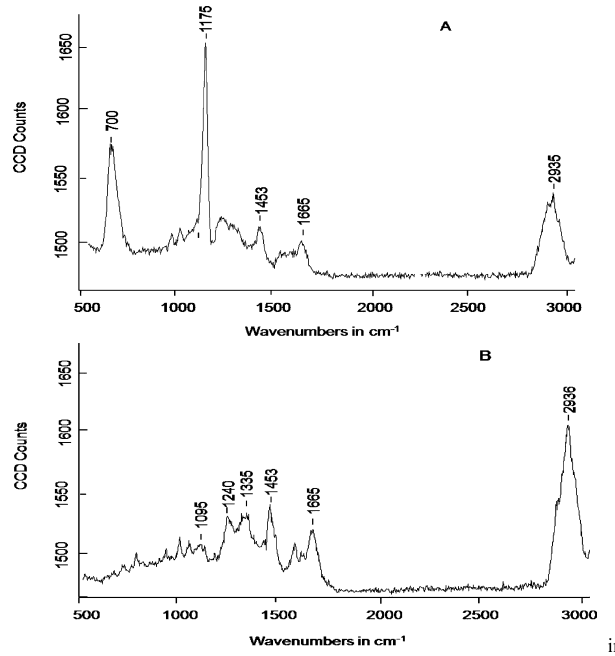

in

FIGURE 2. Raman spectra of (A) a polyphosphate accumulating bacterium with significant amounts of polyphosphate inclusions; (B) a bacterium without polyphosphate inclusions.

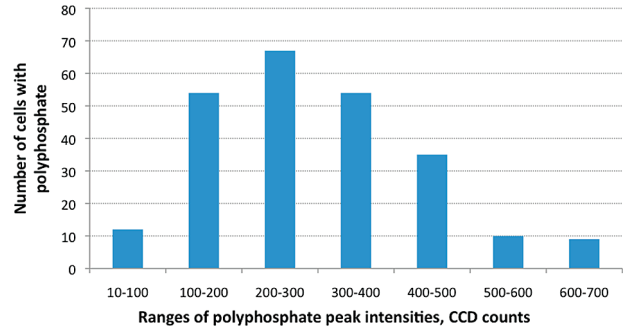

FIGURE 3. Distribution of abundance of cells containing different quantities of intracellular polyphosphate inclusions, including cells identified from multiple phosphate uptake and release tests (number of cells with polyphosphate that are included here is 241).

of the peptide linkage are centered around 1665 cm^{-1}. Their Raman intensities are usually referred to as amide I band. Also significant intensities are caused by C−H waging and scissoring modes around 1453 cm^{-1}, followed by N−C bending vibrations and other C−H deformations between 1400 and 1150 cm^{-1}. PO_2^- vibrations of the DNA phosphate ester backbone and smaller RNA fragments have been reported to appear between 1050 and 1090 cm^{-1}.

Quantification and Variation of Polyphosphate Content in PAO Cells. The polyphosphate band intensities are proportional to the quantity of polyphosphates in the cells. In this study, we used the intensity (CCD counts) of PO_2^- stretching bands occurring at 1168−1177 cm^{-1} as the determinative marker for quantifying the polyphosphates in a given cell because of its greater prominence of peak intensity in comparison with the P−O−P stretches occurring at 690−700 cm^{-1}. Figure 3 shows the histogram of the distribution of the abundance of polyphosphate-containing cells along the ranges of polyphosphate quantities (CCD counts). The plot of the standard normal percentile and the ordered values for polyphosphate intensities approximate a straight line with R^2 value of 0.97 (Figure S1), which indicates a normal distribution (*21*). The individual intracellular polyphosphate quantity ranged from 18 to 686 CCD counts with a

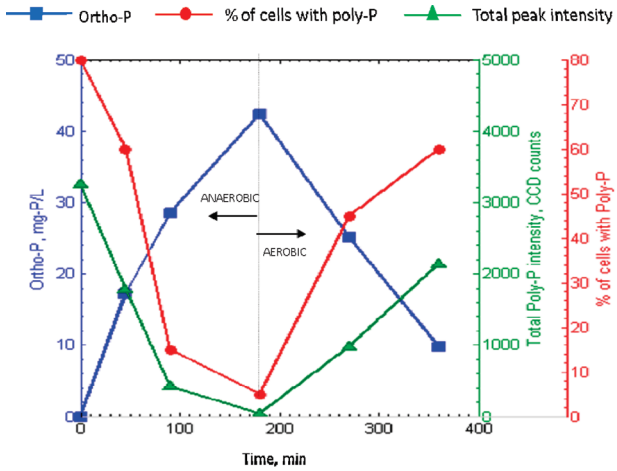

FIGURE 4. Correlation between bulk orthophosphate (ortho-P) concentrations with the proportion of total cells with polyphosphate (poly-P) and the total intensity of polyphosphate in cells quantified with Raman microscopy, during phosphate release and uptake testing.

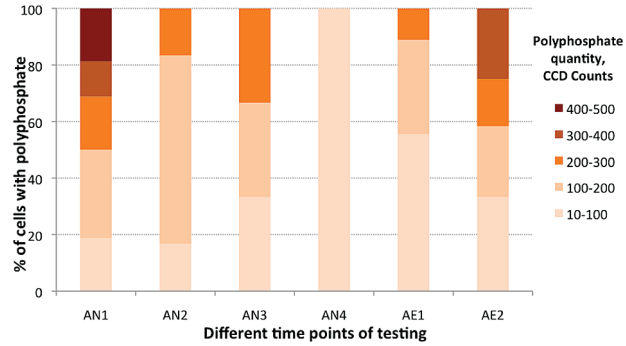

FIGURE 5. Distribution of abundance of cells among different ranges of intracellular polyphosphate quantities (as CCD counts shown in legend) at various time points of anaerobic (AN) and aerobic (AE) phases during the phosphate release and uptake test: AN1 = 0 min in AN phase; AN2 = 45 min in AN phase; AN3 = 90 min in AN phase; AN4 = 180 min in AN phase; AE1 = 90 min in AE phase; AE2 = 180 min in AE phase.

mean value of 292 CCD counts. In this particular EBPR system we studied, the maximum amount of polyphosphate was found to be around 700 CCD, which likely represents the saturation level of polyphosphate for the PAO cells in this system. The saturation level of cellular polyphosphate storage in PAOs is an important parameter in the current EBPR models (*22*). Whether this saturation level varies among different PAOs in various EBPR systems and what factors may affect these saturated polyphosphate levels can be further investigated with the Raman microscopy methods developed here.

Correlation of Phosphate Removal Performance with Abundance of PAO Cells and with Quantities of Polyphosphate Determined by Raman Microscopy. Figure 4 shows the temporal correlation among the orthophosphate concentration measured in solution, the corresponding total intracellular polyphosphate quantity in PAO cells, and the relative abundance of PAO cells in the sludge sample (identified by the Raman method) during an exemplary phosphorus uptake and release test. Under anaerobic conditions, the soluble orthophosphate concentration increases from 0.03 to 42.38 mg/L within 180 min (with a concomitant consumption of 100 mg/L COD) at a rate of 32.8 mg-P/gVSS.h, which is consistent with previous observations with lab-enriched EBPR systems (*23, 24*). The release of phosphate reversely correlated with the percentage of polyphosphate-containing PAO cells, which declined from 80% to 5% (correlation coefficient = −0.96) and with the total polyphosphate intensity in the monitored cells, which decreased from 3648 to 43 CCD. After introducing aerobic conditions, the bulk orthophosphate concentration decreased to 9.69 mg/L within 180 min. Correspondingly, the proportion of cells with polyphosphate accumulations increased from 5% of total bacterial cells at the beginning of the aerobic cycle to 60% after 180 min in the aerobic cycle (correlation coefficient = −0.98) with concurrent increase in the total intracellular polyphosphate intensities from 43 to 2137 CCD. In the anaerobic phase, PAOs hydrolyze the intracellular polyphosphate for energy and release orthophosphate into the solution, which is evidenced by the depletion of cellular polyphosphate and increase in the bulk orthophosphate concentration. Then we observe the replenishment of intracellular polyphosphate content with the introduction of aerobic stage and subsequent reduction of soluble orthophosphate in solution. Figure 4 clearly shows the expected inverse correlation between the temporal bulk orthophosphate measurements and the Raman measurements for total intracellular polyphosphate intensities (summation of polyphosphate intensities for all PAOs observed) obtained in a sample at different time points during the phosphate release and uptake testing (with overall correlation coefficient = −0.97). Thus, the Raman microscopy method developed here is able to capture a statistically reliable number of PAOs present in a sample and the intracellular polyphosphate quantification method is valid. Possible improvement on the methods accuracy with a larger number of sample sizes are being investigated employing an automated microscope stage with an ability to set marker positions.

These results demonstrate that Raman measurements can successfully predict the phosphate release and uptake dynamics in an EBPR system, with quantitative information regarding both the abundance of PAOs and the amount of intracellular polyphosphate at individual as well as population level.

Dynamic Distribution of Polyphosphate Content among Individual Cells during P Release Uptake Test. The polyphosphate band intensities varied considerably from bacterium to bacterium even among those under the same environmental conditions. Figure 5 shows the distribution of PAOs cells with different levels of cellular polyphosphate quantities in samples that were taken at consecutive time points during the phosphate release and uptake test.

Note that at each time point, the percentage of cells with varying polyphosphate contents shown in Y axis is in relevance to the total PAOs that had polyphosphate inclusions and the results here are from the same batch test as shown in Figure 4. Nearly half of the cells with polyphosphate inclusions in the sludge sample (which is taken from the aerobic phase of the continuous flow EBPR reactor), shown as time AN1, were found with relatively higher amount of intracellular polyphosphate (>200 CCD). After 45 min of anaerobic phase after the acetate addition at time zero, cellular polyphosphate depletion was witnessed by the distribution shift to dominance by cells containing much less polyphosphate at time AN2 (<200 CCD). Further extension of anaerobic condition (AN4) resulted in expected complete depletion of polyphosphate and all the cells that had polyphosphate inclusion were left with <100 CCD intensity of polyphosphate. Initiation of aeration led to opposite shifts at AE1 after 90 min, where the distribution of cells in the sample shifted to having more cells with higher polyphosphate levels as a result of aerobic P uptake. And again, the extended aeration for another 90 min seemed to continue the expected shifts to cells with higher polyphosphate content. This distribution is consistent with the continuous increase of total number

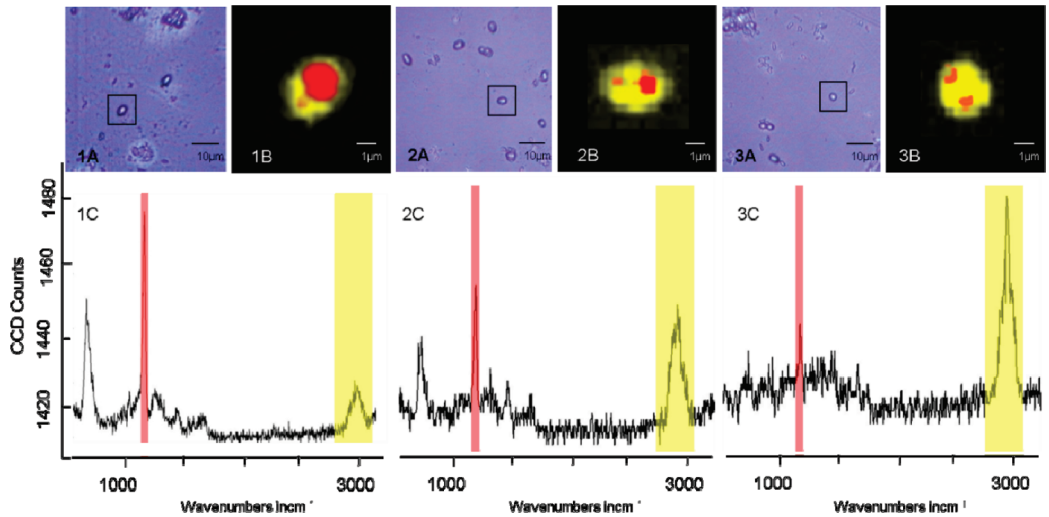

FIGURE 6. High-resolution Raman images of spatial distribution of polyphosphate inclusions inside individual cells. Images (A) are microscopic images taken with a 100x/NA0.9 air objective. Images (B) were reconstructed from Raman intensities between 2800 and 3020 cm^{-1} reflecting the protein density within the bacterium in yellow, and polyphosphate intensities between 1125 and 1225 cm^{-1} showing the polyphosphate distribution within the bacterium in red. The spectra below (C) are representative spectra from the yellow and red regions of the images for protein and polyphosphate intensities, respectively.

of cells containing polyphosphate as well as the total intracellular polyphosphate as the aeration continues (Figure 4).

These results, for the first time, experimentally demonstrated the distributed states of cells in terms of polyphosphate content, even among cells that are exposed to the same experimental conditions. This suggests that agent-based distributive modeling (*22*) will more accurately reflect the behavior of an EBPR process than the traditional average-state based modeling (*25*).

Imaging of Intracellular Polyphosphate in Relevance to Protein Content. Raman spectra can simultaneously capture not only the cellular polyphosphate but also other cellular content such as proteins, as previously explained. In this study, the band between 2800 and 3050 cm^{-1} region (representing C−H stretching vibrations) was used to quantify protein content in cell since organic components exhibit their highest Raman intensities in the C−H stretching region of the spectrum. And this is the most prominent peak among the ones that represent vibration of protein backbones. The size of the bacteria visually identified as PAOs in our system was around 3−5 μm. Given a theoretical microscopic resolution of 430 nm, at the employed laser light, the bacteria are sufficiently large to image the distribution of polyphosphates inside the cytoplasm, based on Raman signal intensities. The theoretical spatial resolution of Raman microscopy is on the same order as conventional optical microscopy. Figure 6-1A is a microscopic picture of a single bacterium. By plotting the Raman intensities of the C−H stretching region, the cell body can easily be reconstructed. In Figure 6-1B, the C−H stretching intensities are shown in yellow, whereas the polyphosphate or PO_2^- intensities are plotted in red. The Raman spectrum in Figure 6-1C is representative of high phosphate concentration from within the red regions of the image where polyphosphate bands dominate over the protein bands. About two-thirds of the cell body is occupied by polyphosphate accumulations suggesting a higher mass percentage from the stored polymers than from the proteins of the cell body. The images 6-2B and 6-3B show the polyphosphate distributions of bacteria with moderate and low amounts of polyphosphate concentrations with lower intensities of the Raman bands associated with polyphosphates as indicated by the spectra in 6-2C and 6-3C. The implication and relevance of this observation can be further revealed with the distribution of intracellular polyphosphate and protein intensities for all the cells analyzed at a specific time point of testing (Figure S2). It shows very clearly that inclusions of polyphosphate in a cell as well as the protein content can vary significantly from cell to cell, indicating distributed state of polyphosphate content among individual cells under the same condition. Furthermore, the images revealed the spatial distribution of polyphosphate inside cells and they showed that the polyphosphates accumulate in smaller or larger aggregates, rather than being evenly distributed within the cytoplasm.

Raman Microscopy for Evaluating Intracellular Polyphosphate in EBPR. The possibility to quantify the number of bacteria that contain polyphosphate as well as their intracellular polymers, which undergo metabolic transition from one form of energy storage to another, is certainly an advantage over techniques that can only evaluate bulk quantities of material. Conventionally, investigation of EBPR mechanisms at cellular levels was impossible because no PAO isolates are currently available and observation of PAOs cells with molecular-based tools such as FISH are only limited to those PAOs that have been identified (studies showed larger diversity of PAOs than current understanding (*17*)). As a result, the dynamics of intracellular polymers can only be inferred indirectly from the bulk measurements of related substrates and individual-cellular-level investigation of EBPR mechanism is very limited. The method developed here offers the opportunity to study the dynamics and thus behavior of an EBPR system in much greater detail and at the cellular level. In the example shown here, the overall temporal courses of the intracellular polyphosphate depletion during anaerobic conditions and recovery during aerobic phase were revealed at both individual and population levels. The findings experimentally demonstrated the variation and distributed states of cells in terms of the quantity of polyphosphate among PAOs even for those under the same environmental conditions. It also revealed that the individual cellular polyphosphate content ranges from zero (no inclusion after depletion of polyphosphate) to a "saturated" maximum level. In addition, the overall polyphosphate depletion or replenishment observed at the overall population level during the phosphate release and uptake phases result from shifts/transition in the

distribution of abundance of PAOs with different amount of polyphosphate inclusions. This implies that the "true" metabolic kinetics for polyphosphate synthesis and consumption by PAOs cells are most likely not in agreement with the "apparent" kinetics determined by measuring the bulk concentrations. The advantage of the Raman method is that it allows for the evaluation of kinetics for cellular polyphosphate metabolism to a very detailed extent and at the cellular level, which will lead to more fundamental and better understanding of the mechanisms of phosphorus removal in EBPR processes.

It would be of potential interest to translate the quantities or intensity ratios of polyphosphate accumulations vs the protein content of a cell quantified by Raman microscopy into more commonly used units such as gram of polyphosphate per unit amount of dried biomass weight. Although Raman spectroscopy has been applied to study concentrations of substance in solutions, it is difficult to establish reliable reference calibrations for a complex system that exhibits an inhomogeneous population and polyphosphate distribution patterns as in our mixed culture EBPR system. Nevertheless, the high correlation coefficient obtained for the expected correlation of changes in phosphate in solution with those quantified in PAOs cells (Figure 4) indirectly demonstrated the accuracy and validity of the Raman microscopy method developed.

In our acetate-fed EBPR system, PAOs accounts for approximately $65 \pm 10\%$ of the total population, among which >60% were *Accumulibacter*-like PAOs based on FISH analysis with the remaining as unidentified PAOs. The results from this study indicate that Raman microscopy analysis can capture nearly all PAOs despite their phylogenetic diversities. The signature of the Raman spectra of polyphosphates seems rather conservative among diverse PAOs in our continuous flow EBPR process. Whether the similar signature Raman spectra of polyphosphate is also conservative among PAOs in different full-scale EBPR systems is under investigation. The peak positions of the P−O−P stretches and PO_2^- vibrations indicate that the predominant fraction of the polyphosphates is present in the form of rather long chain lengths. Furthermore, the Raman spectra of cells do not only show polyphosphate inclusions, but also reveal the presence and quantity of other associated intracellular inclusions and molecules such as poly hydroxy-butyrate (PHB) (*26*) or glycogen, which are relevant in EBPR processes. Our preliminary data indicated that simultaneous observation of polyphosphate and PHB among PAOs and GAOs is possible (Figure S3). Further investigations on how to apply Raman microscopy for evaluating the dynamics of various intracellular polymers and to distinguish and quantify various relevant populations such as PAOs and GAOs involved in the EBPR process are underway.

Acknowledgments

This study was funded by scholarship to ITRI-NU (Industrial Translational Research Initiative at NU) from R&D of AnoxKaldnes Inc. Sweden (now Veolia Water Solutions and Technologies).

Supporting Information Available

Three additional figures for clarification: Figure S1 showing the plot of the standard normal percentile and the ordered values for polyphosphate intensities (normal plot), Figure S2 showing the intracellular distribution of protein and polyphosphate intensities, and Figure S3 showing Raman of pure PHB, a cell with PHB, and a cell with PHB and polyphosphate both. This material is available free of charge via the Internet at http://pubs.acs.org.

Literature Cited

(1) Mino, T.; Van Loosdrecht, M. C. M.; Heijnen, J. J. Microbiology and biochemistry of the enhanced biological phosphate removal process. *Water Res.* **1998**, *32* (11), 3193–3207.
(2) Gu, A. Z. T., I.; Benisch, M.; Stensel, H. D.; Neethling, J. B. The Importance of Modeling Metal Uptake and Release in the EBPR Processes. *Proceeding, WEFTEC 05*; Washington, DC, 2005.
(3) Schonborn, C.; Bauer, H. D.; Roske, I. Stability of enhanced biological phosphorus removal and composition of polyphosphate granules. *Water Res.* **2001**, *35* (13), 3190–3196.
(4) Lindrea, K. C.; Pigdon, S. P.; Boyd, B.; Lockwood, G. A. Biomass characterization in a nitrification-denitrification biological enhanced phosphorus removal (NDBEPR) plant during start-up and subsequent periods of good and poor phosphorus removal. *Water Sci. Technol.* **1994**, *29* (7), 91–100.
(5) Lockwood, G. L., Lindrea, K. C., Seviour, R. J. The distribution of phosphorus and ions in the biological phosphorus removal process. In *Proceedings of the First Australian Conference on Biological Nutrient Removal from Wastewater*, Bendigo, 1990; pp 195−204.
(6) Streichan, M.; Golecki, J. R.; Schon, G. Polyphosphate-accumulating bacteria from sewage plant with different processes of biological phosphorus removal. *FEMS Microbiol. Ecol.* **1990**, *73*, 113–124.
(7) Schlegel, H. G. *General Microbiology*, 7th ed.; Cambridge University Press: Cambridge, 1969.
(8) Kulaev, I. S. *The Biochemistry of Polyphosphates*; Wiley: Chichester, UK, 1979.
(9) Schuster, K. C.; Urlaub, E.; Gapes, J. R. Single-cell analysis of bacteria by Raman microscopy: spectral information on the chemical composition of cells and on the heterogeneity in a culture. *J. Microbiol. Meth.* **2000**, *42* (1), 29–38.
(10) Choo-Smith, L. P.; Maquelin, K.; van Vreeswijk, T.; Bruining, H. A.; Puppels, G. J.; Thi, N. A. G.; Kirschner, C.; Naumann, D.; Ami, D.; Villa, A. M.; Orsini, F.; Doglia, S. M.; Lamfarraj, H.; Sockalingum, G. D.; Manfait, M.; Allouch, P.; Endtz, H. P. Investigating microbial (micro)colony heterogeneity by vibrational spectroscopy. *Appl. Environ. Microbiol.* **2001**, *67* (4), 1461–1469.
(11) Maquelin, K.; Kirschner, C.; Choo-Smith, L. P.; van den Braak, N.; Endtz, H. P.; Naumann, D.; Puppels, G. J. Identification of medically relevant microorganisms by vibrational spectroscopy. *J. Microbiol. Meth.* **2002**, *51* (3), 255–271.
(12) Huang, W. E.; Stoecker, K.; Griffiths, R.; Newbold, L.; Daims, H.; Whiteley, A. S.; Wagner, M. Raman-FISH: combining stable-isotope Raman spectroscopy and fluorescence in situ hybridization for the single cell analysis of identity and function. *Environ. Microbiol.* **2007**, *9* (8), 1878–1889.
(13) Oehmen, A.; Lemos, P. C.; Carvalho, G.; Yuan, Z. G.; Keller, J.; Blackall, L. L.; Reis, M. A. M. Advances in enhanced biological phosphorus removal: From micro to macro scale. *Water Res.* **2007**, *41* (11), 2271–2300.
(14) Schuler, A. J.; Jenkins, D. Enhanced biological phosphorus removal from wastewater by biomass with different phosphorus contents, part I: Experimental results and comparison with metabolic models. *Water Environ. Res.* **2003**, *75* (6), 485–498.
(15) Crocetti, G. R.; Hugenholtz, P.; Bond, P. L.; Schuler, A.; Keller, J.; Jenkins, D.; Blackall, L. L. Identification of polyphosphate-accumulating organisms and design of 16S rRNA-directed probes for their detection and quantitation. *Appl. Environ. Microbiol.* **2000**, *66* (3), 1175–1182.
(16) Amann, R. I.; Binder, B. J.; Olson, R. J.; Chisholm, S. W; Devereux, R.; Stahl, D. A. Combination of 16S rRNA-targeted oligonucleotide probes with flow cytometry for analyzing mixed microbial populations. *Appl. Environ. Microbiol.* **1990**, *56*, 1919–1925.
(17) Gu, A. Z.; Saunders, A.; Neethling, J. B.; Stensel, H. D.; Blackall, L. L. Functionally relevant microorganisms to enhanced biological phosphorus removal performance at full-scale wastewater treatment plants in the United States. *Water Environ. Res.* **2008**, *80* (8), 688–698.
(18) Jager, H. J. D.; Heyns, A. M. Study of the hydrolysis of sodium polyphosphate in water using Raman spectroscopy. *Appl. Spectrosc.* **1998**, *52* (6), 808–814.
(19) Corbridge, D. E. C.; Lowe, E. J. The infra-red spectra of some inorganic phosphorus compounds. *J. Chem. Soc.* **1954**, 493–502.
(20) Naumann, D. FT-infrared and FT-Raman spectroscopy in biomedical research. *Appl. Spectrosc. Rev.* **2001**, *36* (2−3), 239–298.
(21) Ajit C. Tamhane, D. D. *Statistics and Data Analysis: From Elementary to Intermediate*; Prentice Hall, 1999.

(22) Schuler, A. J. Diversity matters: Dynamic simulation of distributed bacterial states in suspended growth biological wastewater treatment systems. *Biotechnol. Bioeng.* **2005**, *91* (1), 62–74.
(23) Monti, A.; Hall, E. R.; Koch, F. A.; Dawson, R. N.; Husain, H.; Kelly, H. G. Toward a high-rate enhanced biological phosphorus removal process in a membrane-assisted bioreactor. *Water Environ. Res.* **2007**, *79* (6), 675–686.
(24) Liu, W. T.; Nakamura, K.; Matsuo, T.; Mino, T. Internal energy-based competition between polyphosphate- and glycogen-accumulating bacteria in biological phosphorus removal reactors - Effect of P/C feeding ratio. *Water Res.* **1997**, *31* (6), 1430–1438.
(25) Henze, M. *Activated Sludge Models: ASM1, ASM2, ASM2d and ASM3*; IWA Scientific and Technical Report: London, 2000.
(26) De Gelder, J.; Willemse-Erix, D.; Scholtes, M. J.; Sanchez, J. I.; Maquelin, K.; Vandenabeele, P.; De Boever, P.; Puppels, G. J.; Moens, L.; De Vos, P. Monitoring poly(3-hydroxybutyrate) production in Cupriavidus necator DSM 428 (H 16) with Raman spectroscopy. *Anal. Chem.* **2008**, *80* (6), 2155–2160.

ES900251N